Chemical Engineering Journal 401 (2020) 126093

Contents lists available at ScienceDirect

Chemical Engineering Journal

journal homepage: www.elsevier.com/locate/cej

High-temperature dielectric polymer nanocomposites with interposed montmorillonite nanosheets

Yifei Wang[a], Zongze Li[a,b], Chao Wu[a], Yang Cao[a,b,*]

[a] Electrical Insulation Research Center, Institute of Materials Science, University of Connecticut, 97 N Eagleville Rd, Storrs, CT 06269, USA
[b] Department of Electrical and Computer Engineering, University of Connecticut, 371 Fairfield Way, Storrs, CT 06269, USA

HIGHLIGHTS

- A sandwiched BT/PAI nanocomposite reinforced by 2D MMT interfaces is proposed.
- A high energy density of 3.6 J cm^{-1} with an efficiency of 70% is achieved at 150 °C.
- The anisotropic conductivity of MMT regulates the charges transport along in-plane.

GRAPHICAL ABSTRACT

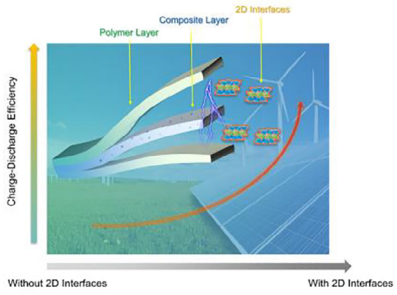

ARTICLE INFO

Keywords:
Dielectrics
Energy storage
Efficiency
2D materials
Interfaces

ABSTRACT

Over the past decades, energy densities have always been considered as the key factors for realizing compact and highly efficient dielectric polymer capacitors. However, high-energy-density polymer dielectrics are limited by insurmountable drawbacks of high energy loss and low charge-discharge efficiency, which are far behind the industrial requirement for application under high temperature/voltage working conditions. Herein, a versatile method to suppress the energy loss of polymer dielectrics is presented, whereby two-dimensional montmorillonite nanosheets are interposed at the interfaces of a sandwich-structured barium titanate/polyamideimide film. The anisotropic electrical conductivity of the nanosheets provides paths to relationally regulate the charges transport along the in-plane direction while suppressing the through-plane conduction. As a result, nearly 50% of the energy loss can be eliminated with an applied electric field of 400 MV m^{-1} at 150 °C, thus leading to a ~100% enhancement of energy density (3.6 J cm^{-1}), accompanied with a high charge-discharge efficiency of 70%, which outperforms all commercial high-temperature polymers. This work uncovers an effective and scalable pathway to enable high-density dielectric energy storage applicable to a wide range of polymer dielectrics at harsh operating conditions while promoting mechanism understanding of interfaces for interfacial engineering of high-performance dielectrics.

1. Introduction

Electrostatic capacitors (EC), which possess the highest power density among all energy storage devices, have become an indispensable part in the rapid developing electronic and electrical industries, typically for high-frequency power inverter, pulsed power

* Corresponding author at: Electrical Insulation Research Center, Institute of Materials Science, University of Connecticut, 97 N Eagleville Rd, Storrs, CT 06269, USA.
E-mail address: yang.cao@uconn.edu (Y. Cao).

https://doi.org/10.1016/j.cej.2020.126093
Received 21 April 2020; Received in revised form 2 June 2020; Accepted 24 June 2020
Available online 30 June 2020
1385-8947/

generation, and energy storage devices [1–5]. As the key component in electrostatic capacitors, polymer dielectrics have evident advantages of high electrical breakdown strength, mechanical flexibility, low cost, and great reliability, compared with inorganic ceramic counterparts [6–8]. Yet, the ECs have energy densities severely lower than those of electrochemical devices, such as batteries and supercapacitors, and therefore currently stem as the largest components in power inverter/converters measured by either volume or weight [9]. For example, biaxially oriented polypropylene (BOPP), the state-of-the-art commecially available dielectric polymer, can only deliver a low energy density of ~2 J cm^{-3} with limited cycle life.

The energy density stored in a dielectric material (U_e) is determined by the electric displacement (D) and applied electric field (E) as $U_e = \int E\mathrm{d}D$, where D is related to the dielectric permittivity (ε_r) by $D = \varepsilon_0\varepsilon_r E$, indicating that the maximum stored energy density in a dielectric material is governed by its ε_r and the maximum applicable electric field [10]. Although polymers are favorable electrical insulating materials with high electric field tolerance, their U_e is generally limited by their low ε_r [11,12]. For this reason, the forthright composite approach has been employed by introducing ceramic nanofillers into the polymer matrix. Normally, ceramics with high ε_r are favorable enablers for the nanofillers, and ferroelectric polymers, such as poly(vinylidene fluoride) (PVDF) and its co-polymers, are adopted as high-ε_r matrix [13–16]. Nevertheless, it is worth noting that the hysteresis from ferroelectric polymers and the electrical conduction from ceramic nanofillers would contribute to high energy loss in polymer nanocomposites during charge-discharge process, leading to a low charge-discharge efficiency (η) (defined in Fig. S1) that significantly limits their service time, reliability, and energy consumption characteristics for practical applications.

Such paradox between high U_e and high η in polymer dielectrics has been well-recognized, while, more notably, this ambivalent relationship will intensify towards high-temperature working conditions, which raises greater challenges for their practical applications [17–19]. For example, PVDF based nanocomposites exhibit the highest energy density (> 20 J cm^{-3}) among all polymer dielectrics at ambient environment, but their operating temperature is limited to below 50 °C because of the dramatic drop of η to as low as ~20% at 100 °C [20]. So as to BOPP, widely recognized as the benchmark dielectric material for the drivetrain of electric vehicles, holds high η of more than 90% from room temperature to 85 °C, but would fail completely at temperatures higher than 105 °C, thereby requiring often a secondary cooling system to decrease the busbar temperature in vehicle powertrain system [21]. To address this issue, one tentative solution is to replace the polymer matrix with high glass transition temperature (T_g) polymers, such as polyetherimide (PEI), fluorine polyester (FPE), polycarbonate (PC), polyimide (PI, Kapton), and poly(ether ether ketone) (PEEK) [22]. However, it is found that benzene rings located in the backbones of these high-T_g polymers could introduce π bonding energy levels that may lower the band gap and thus lead to energy loss increment at high electric field (> 300 MV m^{-1}) [23,24]. Consequently, to maintain an acceptable η, only a moderate electric field can be applied on these aromatic polymer dielectrics for long-term charge-discharge service, which limits their energy densities to within 2 J cm^{-3} in most previous studies.

The emerging of layer-structured design inaugurates a neoteric approach to fundamentally suppress the energy loss and improve the η of polymer dielectrics [25–29]. Wang and co-workers presented a sandwich-structured ceramic/polymer nanocomposite by inserting a pure polymer layer in the middle of two composite layers containing high-ε_r ceramic nanoparticles, where an enhanced η is achieved through compositional tailoring. It has been demonstrated that low-electric-field regions are formed in this layered structure that will impede the charge transport across the polymer film, leading to dramatically suppressed electrical conductivity and energy loss [30,31]. Furthermore, it is found that those barrier regions are located at the interfaces between layers with different electric constitutive parameters (i.e., dielectric permittivity and electrical conductivities), acting as interfacial barriers. More recently, such enhancement of η in layered dielectrics is also realized in high-temperature ceramic/polymer nanocomposites, where the layered structure can effectively restrain the electrical conduction of ceramic nanofillers, giving rise to high U_e accompanied with high η even at 150 °C [32].

Despite the fact that the significant role of interfaces has been generally recognized, few studies are directly focusing on interfacial modification through nano-scale engineering. Such a lack of interfacial engineering studies also limits the mechanism understanding of interfacial effect. Here, we present and demonstrate a novel design strategy to suppress the energy loss and improve the charge-discharge efficiency of polymer dielectrics by constructing and manipulating two-dimensional (2D) interfaces, a scheme generally applicable to all layer-structured polymer composites. In detail, one high-ε_r barium titanate/polyamideimide (BT/PAI) composite layer is clamped between two pure PAI layers, where their interfaces are interposed with montmorillonite (MMT) nanosheets with anisotropic electrical conductivity. PAI is adopted as the polymer matrix due to its high T_g, good processability, and favorable characteristics in high-temperature and -field resistances [33]. (Molecular structure of PAI is shown in Fig. S2) Film casting via doctor blading facilitates the orientation of 2D materials, thus paving conduction pathways along the in-plane direction and reducing the leakage current through the thickness direction. Plausible charges dissipation at the MMT interfaces is verified by both electrical characterization and finite element simulation. This current regulating effect via the 2D interfaces becomes more apparent at high temperature up to 150 °C, endowing a 36% decrease of energy loss at a high electric field of 400 MV m^{-1} when compared with that of the counterparts without interfacial reinforcement, and resulting in eventually an ultrahigh effective discharged energy density of 3.6 J cm^{-3} accompanied with a favorable charge-discharge efficiency of 70%, outperforming all the state-of-the-art high-temperature polymers. The advantages of interfacial modification are further highlighted when a larger amount of high-ε_r BT nanoparticles (40 wt%) is introduced in the layered nanocomposites, showing a 45% lower energy loss and a 52% enhanced charge-discharge efficiency. The processability of the interface manipulation method presented here ensures its applicability to all solution-processed polymers, providing a promising enabler for exploring high-U_e and high-η reliable dielectric nanocomposites.

2. Experimental section

2.1. Fabrication of layered polymer nanocomposites with 2D interfaces

The layered samples were prepared by a combined doctor blade casting/spray coating technology layer-by-layer. For the precursor of the middle layer composed of BN/PAI, BT nanoparticles (100 nm, Acros Organics) were dispersed in DMF (Fisher Chemical) by tip-type sonication for 20 min, which was then mixed in the required ratio with PAI resin (Tritherm® A981-H-25, Elantas Eletrical Insulation) and stirred overnight. The mixture was then processed by tip-type sonication for 10 min just before casting. The pure PAI solution for outer layer casting is subjected to an one-step stirring with DMF as the solvent. For the spraying precursor, MMT nanosheets (BYK Additives Inc.) were exfoliated and dispersed in DMF by tip-type ultrasonication for 1 h (50 W), and then PAI resin was mixed into the solution by magnetic stirring as the binders for the nanosheets. The weight ratio of MMT and PAI is 1:4, while the total solid part (MMT + PAI) content is 4 wt%.

First, a layer of PAI was cast on a glass substrate by doctor blading. After drying at 80 °C for 10 min, MMT interface was sprayed on the top of the PAI layer. The thickness of the interface can be simply tuned by controlling the spraying times. After drying under ambient condition for 10 min, the middle layer of BT/PAI was cast on the spraying interface. Again, after drying, the other interface and the top layer were

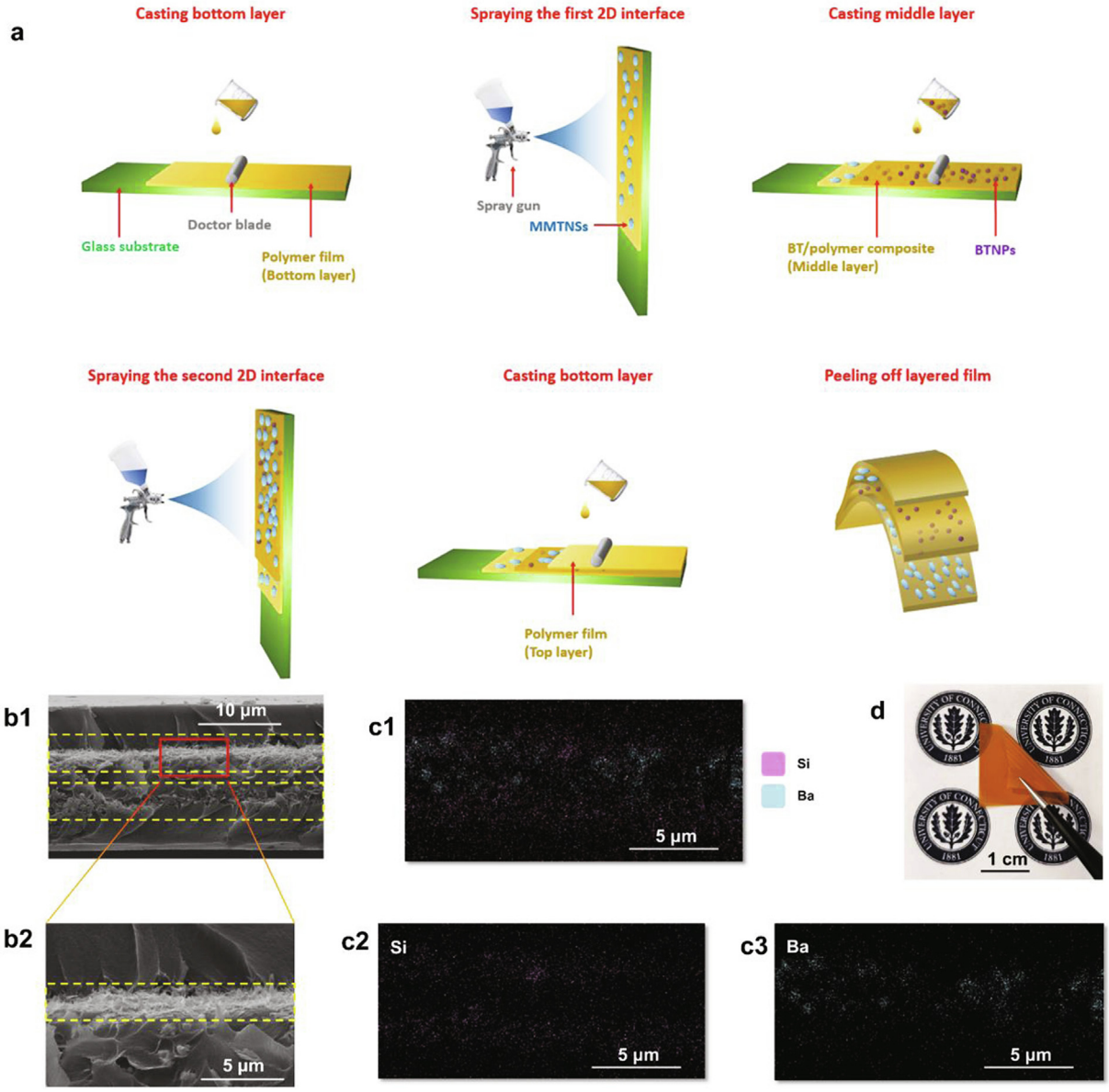

Fig. 1. (a) Schematic of the fabrication process of the interface reinforced layered polymer nanocomposites. (b) Cross-sectional SEM images and c) EDAX results of the MMT interface reinforced BT/PAI layered polymer nanocomposites. (d) Photograph of the MMT interface reinforced BT/PAI layered polymer nanocomposites.

sprayed and then cast, respectively. Afterwards, the layered film was dried at 130 °C overnight to completely remove the solvent, which was followed with curing at 300 °C for 2 h in a vacuum oven. The layered nanocomposite was peeled from glass for a free-standing film, whose thickness was carefully controlled to 10 ~ 15 μm.

2.2. Characterization

The morphologies of layered nanocomposites were characterized by scanning electron microscopy (SEM) and energy dispersive x-ray analysis (EDAX) (FEI Teneo LVSEM). The X-ray diffraction analysis was conducted by a Bruker D2 diffractometer with a LynxEye linear detector for high-speed data collection. Gold/palladium (Au/Pd) electrodes were sputtered on both sides of prepared layered films (6002-8 Ted Pella, Inc.) for the measurement of dielectric properties. The thickness of each electrode point is measured by MeasureItAll Model LE1000-2 thickness gauge. Dielectric permittivity and dielectric loss were characterized by impedance analyzer (Solartron 1260) and resistance meter, covered a frequency range of 1 Hz ~ 10 kHz, as well as a temperature range of 20 ~ 180 °C. Electric displacement-electric field (*D-E*) loops measured at 100 Hz with a modified Sawyer-Tower circuit. High electric field conduction was carried out with a lab-designed capacitive cancellation measurement system. A dynamic gain controlled negative feedback loop was utilized to cancel the capacitive current, and the signal output reflect the time integrated conduction current. The electrical surface resistance was measured by a high resistance meter (Hewlett Packard, 4329A). A high voltage of 1 kV was applied for 30 s to charge the samples, and the surface resistance was recorded after another 10 s saturation.

2.3. Finite element modeling (FEM)

The electric potential, electric field distribution, space charge distribution, and leakage current density of the layered films with nanoscale interfaces were simulated by using FEM. The size of the constructed model is 12.4 × 4 μm^2, composed of three layers with 4 μm thick and two interfaces with 0.2 μm thick, respectively. A voltage of 5 kV was applied on the top of the model and the bottom was grounded.

The dielectric permittivity of PAI, BT, and MMT were endowed for 4.5, 2000, and 500, respectively. The conductivity of PAI and BT were 10^{-15} S m^{-1} and 10^{-11} S m^{-1}, respectively. To mimic the anisotropic electrical properties of MMT, a high surface conductivity of 10^{-3} S m^{-1} was adopted, compared with the bulk conductivity of 10^{-8} S m^{-1} [34,35].

The space charge density (ρ) in the polymer composite film is governed by Ohm's law, the equation of continuity, and Gauss's law, as presented by:

$$\frac{\partial \rho}{\partial t} + \frac{\sigma}{\varepsilon}\rho = 0$$

This equation has the solution:

$$\rho(t) = \rho_0 e^{-t/\tau}$$

where t is the eternal time scale, $\tau = \varepsilon/\sigma$ is the charge relaxation time, ε is the dielectric permittivity, and σ is the electrical resistivity. In this study, we assume t is long enough, and a stationary solution can be achieved.

3D models combined with Charged Particle Tracing (CPT) Module were further developed to evaluate the charge regulation effect of 2D MMT interfaces. The size of the 3D models is 1 × 1 × 12.4 μm^3, composed of three layers with 4 μm thick and two interfaces with 0.2 μm thick, respectively. An electric potential is applied on the top surface, and the bottom surface is grounded. Electrons are assumed as the injected charged particles with charges of -1.60×10^{-19} C and masses of 9.11×10^{-31} Kg. Ten charged particles were randomly injected from a circle region with a diameter of 0.5 μm in each 3D model, locating at the center of the bottom surface. The charged particles move toward the top electrode driven by the electric force which is deduced by the distribution of electric field. Time dependent particle trajectories can be simulated with specified time range.

3. Results and discussion

The manufacturing process of the 2D interfaces reinforced layered BT/PAI nanocomposite is illustrated in Fig. 1a. Note that the spraying precursor with a 4 wt% solid (MMT + PAI) weight content was carried to ensure a low viscosity for achieving desirably oriented MMT in the in-plane direction assisted by gravity driven flow orientation [36]. Free-standing films can be obtained with this manufacturing technique, and the flexibility and large-scale processability of the films are evidenced in Fig. 1d and Fig. S3. Fig. 1b displays the cross-sectional scanning electron microscopy images of the synthesized 2D layered film. The wrinkles at the interfaces adjacent to the middle layer observed in Fig. 1b1 are characteristic of 2D MMT. To further confirm the layered structure, EDAX technique was carried out and shown in Fig. 1c, and the positions of MMT (represented by Si element) and BT (represented by Ba element) were highlighted, according to which, a belt of Ba outlined by blue dots locates in the middle, sandwiched in two MMT zones (red dots). For this specific sample, the MMT interfaces with a thickness of 2 μm were realized by 10-times spraying to clearly distinguish the interfaces. The thickness of the interface goes quasi-linearly with the number of sprays, with each nano-scaled 2D MMT layer measuring ~200 nm in thickness (as shown in Fig. S5-6). Detailed morphology of BT and MMT powders can be found in Fig. S7.

Three different layered nanocomposites (1) without MMT interfaces; (2) with nano-scale 2D MMT interfaces (1-time spraying); (3) with micro-scale MMT interfaces (10-times spraying) were then prepared for dielectric characterization, which are hereafter termed as PBP, PMBMP-1L, and PMBMP-10L, respectively. After interposing nano-scale MMT interfaces, the real part of dielectric permittivity (ε_r) appears to be unaffected (Fig. 2a), while, in the meantime, a suppressed dielectric loss can be found in PMBMP-1L in a wide range of frequency (Fig. 2b), potentially beneficial for achieving small leakage current and low energy loss. The dielectric loss then inversely increases with the increment of interfaces thickness to micrometer scale, reflecting the dimensional sensitivity of MMT interfaces to dielectric properties. At higher electric field, a lower maximum polarization (P_{max}) and a higher remnant polarization (P_r) in PMBMP-10L could be distinguished in the electric displacement-electric field (*D-E*) loops (Fig. 2c), implying the suppressed energy storage ability. The difference between P_{max} and P_r represents the energy releasing efficiency, and the highest value of P_{max}-P_r (~1.9 μC cm^{-2}) is achieved in PMBMP-1L compared with that of PBP at 400 MV m^{-1}, as seen in Fig. 2d. With 2 μm thick MMT interfaces, a marked increment of P_r can be observed in PMBMP-10L, in which MMT nanosheets with anisotropic electrical conductivity, i.e. highly conductive surface, could contact each other edge-to-edge to form a conductive 3D network, thus elevating the through-thickness conductive loss. Evidently, both low dielectric loss and large value of P_{max}-P_r uncover the loss suppression characteristics of nanoscale MMT interfaces, which may endow PMBMP-1L with favorable dielectric energy storage properties.

Fig. 3a evaluates the temperature dependent ε_r of the layered nanocomposites from room temperature to 180 °C. A minor variation in ε_r, that is, < 5%, could be observed in all the three films in a wide range of temperature. Two small peaks locating at ~40 °C and > 180 °C stem from the polarization processes of PAI and BT, respectively. Concurrently, the dielectric loss first increases and then decreases with the increment of temperature. It is also evident that appreciably suppressed dielectric loss can be seen in PMBMP-1L, compared with other two counterparts (Fig. 3b). For example, the highest value of dielectric loss obtained at ~90 °C is still lower than 1%, compared to 1.1% and 1.15% for PBP and PMBMP-10L, respectively. Energy losses are deduced from temperature/electric field dependent D-E loops (Fig. S8), by integrating the area inside the loops, as presented in Fig. S9 (at 300 MV m^{-1}) and Fig. 3c (at 400 MV m^{-1}) (electric field dependent energy loss shown in Fig. S10). Apparently, a much decreased energy loss can be achieved by interposing nanoscale MMT interfaces into the layered nanocomposites, especially at high electric field/temperature. For example, at 400 MV m^{-1} and 150 °C, PBP exhibits an energy loss of 2.5 J cm^{-3}, whereas the loss of PMBMP-1L is only 1.6 J cm^{-3}. Charge-discharge efficiency (η) has been studied and summarized in Fig. 3d (electric field dependent η shown in Fig. S11). PMBMP-1L outperforms other layered nanocomposites, possessing a remarkable η approaching 70% even at harsh environment (400 MV m^{-1} and 150 °C), which is 10% and 30% higher than that of PBP and PMBMP-10L, respectively. Such improvement of η can contribute to an enhanced discharged energy density, as shown in Fig. 3e. The energy storage performance of PMBMP-1L has been evaluated along with state-of-the-art high temperature polymers including PEI, FPE, PC, Kapton, PEEK, and polyimide-based nanocomposites (Fig. 3f) [15,37–39]. The layered nanocomposite with nanoscale 2D interfaces shows overwhelming superiority to all commercial polymers at 150 °C. PMBMP-1L can discharge 3.6 J cm^{-3} at 400 MV m^{-1}, which is twice that of PEI, accompanied by a comparative η value. Remarkably, its discharged energy density can be further raised to 4.6 J cm^{-3} at an increased electric field of 450 MV m^{-1}. These results indicate that, by replacing BOPP with PMBMP-1L, the volume of power converts in electric vehicle could be reduced by half and existing cumbersome cooling systems can be completely eliminated; let alone, BOPP possesses a low energy density of only ~2 J cm^{-3} at a low temperature of 85 °C.

The pronounced suppression in energy loss and enhancement in discharge efficiency from the 2D interfaces reinforced layered composites have been further studied by using finite element simulation. Fig. 4a describes the electric field distribution of the layered films, deduced by the electric potential pattern (Fig. S12a). It can be seen that the electric field is elevated around the BT nanoparticles due to the large contrast of ε_r between polymer matrix and ceramic fillers. The region with high electric field stems from charges accumulation at local interfacial area [40]. Conductive paths are assumed to be formed when the distance between adjacent particles is not long enough since their

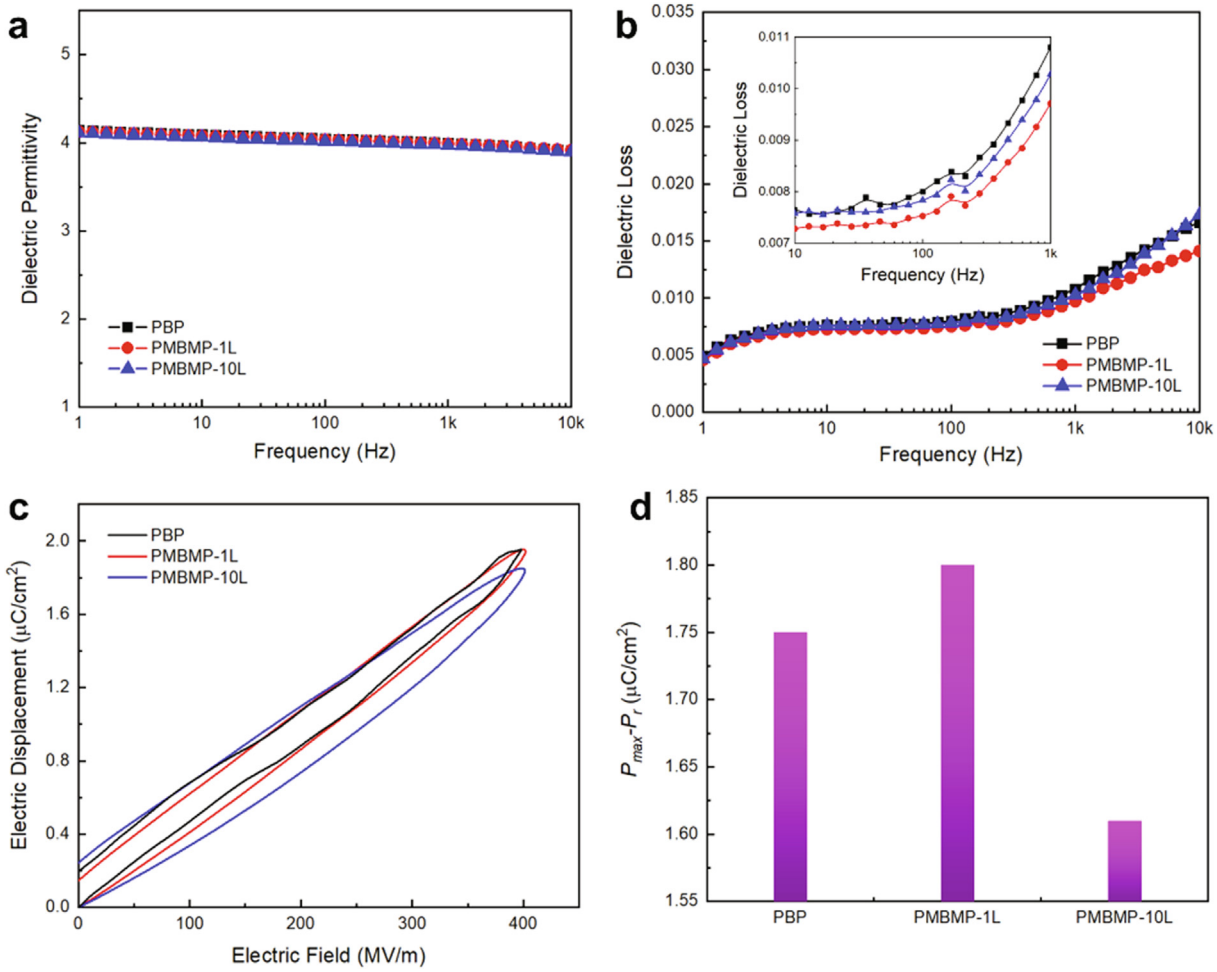

Fig. 2. The dependences of (a) dielectric permittivity and (b) dielectric loss on frequency for PBP, PMBMP-1L, and PMBMP-10L layered nanocomposites. (c) Unipolar *D-E* loops of PBP, PMBMP-1L, and PMBMP-10L layered nanocomposites at room temperature. (d) The differential value of maximum polarization and remnant polarization of PBP, PMBMP-1L, and PMBMP-10L layered nanocomposites at 400 MV m^{-1}.

interfacial area could overlap to each other [41]. On the contrary, alleviated electric field is presented in proximity to the MMT nanosheets due to their moderate ε_r and 2D morphological characteristics. As presented in Fig. 4b, large densities of positive and negative charges can be found below and above BT nanoparticles, respectively, while those are much smaller on the surfaces of MMT nanosheets. It is worth noting that MMT can "rectify" the leakage current by regulating the direction of leakage current from out-of-plane (*y* axis) to in-plane (*x* axis) direction (inset Figures of Fig. 4c and Fig. S12b), as its conductive surfaces provide paths for charges dissipation. As for the case with BT nanoparticles, although the current flow direction is altered when it approached the nanoparticles because of heterocharges attraction or homocharges repulsion, the net leakage current along x axis is close to zero due to the fact that the distorted currents around the isotropic nanoparticles could compensate with each other. The value of $J_x/(J_x - J_y)$ is utilized to describe the effectiveness of current regulating, where J_x and J_y represent the x- and y-component of leakage current density, respectively. We took all grid points in the MMT and BT containing composite layers into consideration and summarized the average value of the simulated leakage current densities in Fig. 4c. The MMT phase shows a strong current suppressing effect by regulating 4.6% of the total leakage current from *y* to *x* direction, which is 46 times higher than that of BT containing layer, leading to a significantly suppressed J_y. This indicates that introducing oriented 2D MMT interfaces efficiently blocks charges transport through the dielectric films while regulating them to dissipate along the in-plane direction, which can be evidenced by the reduced electrical surface resistance of the polymer with 2D MMT coating (Fig. S13). For PMBMP-10L, larger amount of charges could diffuse to create a dispersive region much larger than the capacitive area covered by electrodes. In this case, not all charge signals can be collected from the electrodes during dielectric measurements, leading to undervalued capacitance and polarization, as well as conduction, thus delivering a depressed D-E loops and energy loss (Fig. 3d and Fig. S8c). To elucidate the conduction behavior globally, pre-breakdown integral conduction current measurement has been carried out on the layered nanocomposites by using a dynamic gain controlled capacitive cancellation circuitry, as shown in Fig. 4d and Fig. S14. With electric field increasing, turning points (TP) can be found existing in all films, where the current starts to increase dramatically. Owing to the current regulating effect of MMT, the leakage current of PMBMP-1L is significantly suppressed, thus contributing to a rightward shift of TP, from 322 MV m^{-1} in PBP to 380 MV m^{-1}, at 150 °C. The decreased leakage current is believed as the origin of low energy loss, resulting in pronouncedly enhanced charge-discharge efficiency and energy density at high temperature/electric field conditions.

The charge regulation effect of the 2D MMT interfaces is enabled by local anisotropic electric conductivity, which can be further identified by simulating the charged particles trajectories in 3D models, as shown in Fig. 5a and b. Ten charged particles are injected with random positions from an inlet with a diameter of 0.5 μm, transporting towards the top electrode under the electric field. In PMBMP-1L with MMT

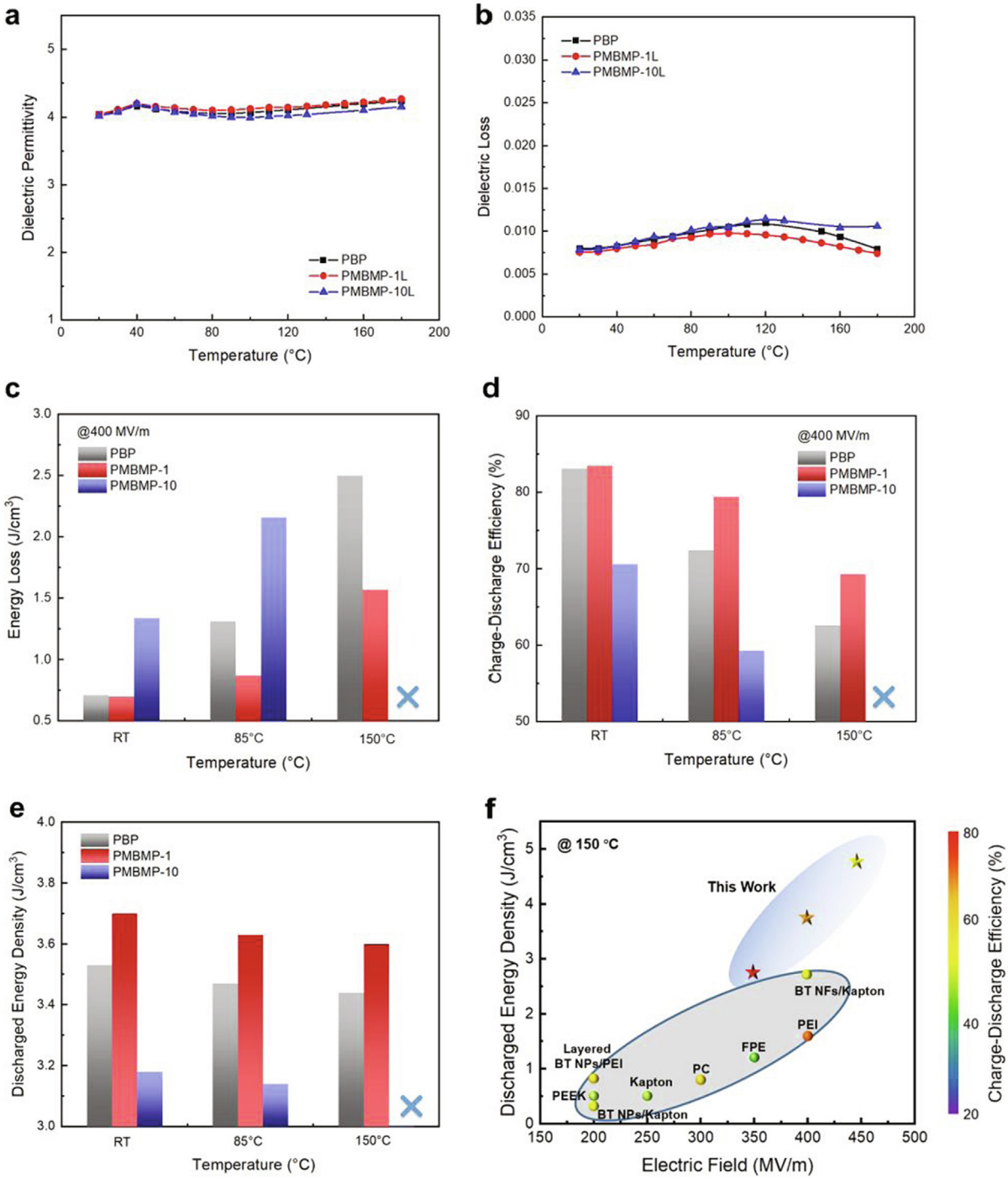

Fig. 3. The dependences of (a) dielectric permittivity and (b) dielectric loss on temperature for PBP, PMBMP-1L, and PMBMP-10L layered nanocomposites. (c) Energy losses, (d) charge-discharge efficiencies, and (e) discharged energy densities of PBP, PMBMP-1L, and PMBMP-10L layered nanocomposites at an applied electric field of 400 MV m^{-1}. PMBMP-10L fail at 150 °C. (f) Comparison of discharged energy density and charge-discharge efficiency (indicated by the color of data point) of PMBMP-1L with that of state-of-the-art high-temperature polymers and PI family nanocomposites [15,37–39].

interfaces, the charged particles tend to diverge along the radial direction. Although the particle trajectories in PBP are not straight lines due to the distorted electric field around BT nanoparticles (Fig. S15), it shows higher convergence compared with that in PMBMP-1L. The charged particle divergence can be quantitatively analyzed by comparing the initial and end positions of the particles (Fig. 5c–e). It can be seen that the distance between the two furthest particles in PBP changes from 0.44 to 0.65 μm, while that in PMBMP-1L shows a more apparent increase from 0.43 to 0.68 μm, suggesting the charged particles can be regulated to transport along the in-plane direction with the existence of MMT interfaces.

We then prepared a series of layered nanocomposites by monotonously increasing the BT content in the middle layer from 15 wt% to 40 wt%. The function of MMT interfaces to restrain energy loss has been more clearly manifested in the film with larger amount of high-ε_r ceramic particles that induce enhancement of electrical conductivity. For example, no distinct difference of energy losses can be found between PBP and PMBMP-1L films with BT content lower than 20 wt%, while, however, the energy loss can be suppressed by 45% with ceramic content increased to 40 wt% at 250 MV m^{-1} and 150 °C, which thereby

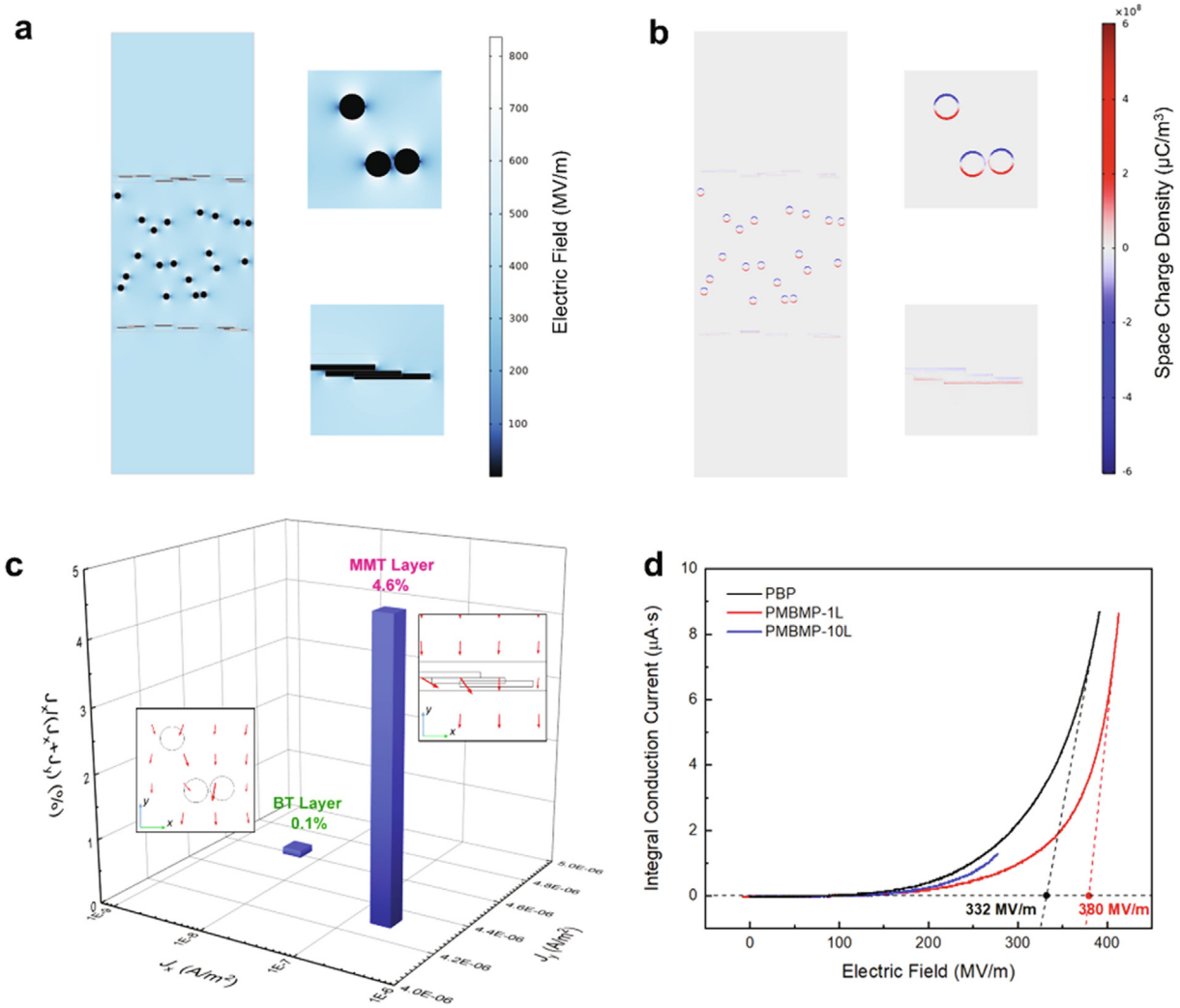

Fig. 4. (a) The electric field distribution and (b) space charge distribution of PMBMP-1L. (c) The average value of leakage current densities along in-plane (J_x) and out-of-plane (J_y) directions and the content of J_x in MMT and BT contained layers, respectively. Inset: The distribution of leakage current density around BT nanoparticles and MMT nanosheets, respectively. The absolute value and the direction of leakage current are indicated by the red arrows proportionally. (d) Integral conduction currents with the increment of electric field in PBP, PMBMP-1L, and PMBMP-10L layered nanocomposites at 150 °C. (For interpretation of the references to color in this figure legend, the reader is referred to the web version of this article.)

provokes a significant enhancement of 52% for charge-discharge efficiency (Fig. 6, *D-E* loops shown in Fig. S16). It is important to note that BT nanoparticles with high conductivity could introduce remarkable energy loss in traditional layered polymer films [42], which can be effectively limited in the newly designed composite with 2D MMT interfaces, delivering a relatively stable charge-discharge efficiency with BT content increasing (Fig. S17).

4. Conclusion

In summary, a facile and versatile approach to reinforce layered polymer nanocomposites with 2D interfaces towards high-temperature dielectric energy storage has been demonstrated in this work by interposing nanoscale MMT between adjacent layers. Different from traditional layered films, this novel designed nanocomposite with tailored thickness of 2D interfaces is capable of significantly suppressing dielectric loss and energy loss at elevated temperature, yielding highly enhanced charge-discharge efficiency and energy density surpassing all commercial polymer films at 150 °C. The MMT interfaces could impede the charge penetration through whole film and regulate leakage current dissipating along the in-plane direction for low conduction loss. An ultrahigh energy density of 3.6 J cm^{-3} accompanied with a η of 70% has been realized in the interface reinforced layered nanocomposites at 150 °C and 400 MV m^{-1}, which is at least two times higher than that of state-of-the-art high-temperature polymers, e.g., PEI, under the same conditions. More notably, the advantages of MMT interfaces can be further carried forward when larger amount of BT nanoparticles are introduced for high ε_r. The energy loss and η are depressed and improved by 45% and 52%, respectively, after inserting MMT interfaces into a sandwiched film with 40 wt% BT in the middle layer. The structure optimization by introducing 2D interfaces with anisotropic materials into layered polymer nanocomposites provides a new paradigm to explore low loss, high efficiency, high energy density dielectric materials and devices for harsh environment.

Declaration of competing interest

There are no conflicts to declare.

Acknowledgements

This work is supported through the NSF Phase I i/UCRC University of Connecticut Site: Center for Novel High Voltage/Temperature Materials and Structures (NSF HVT) (1650544) and the

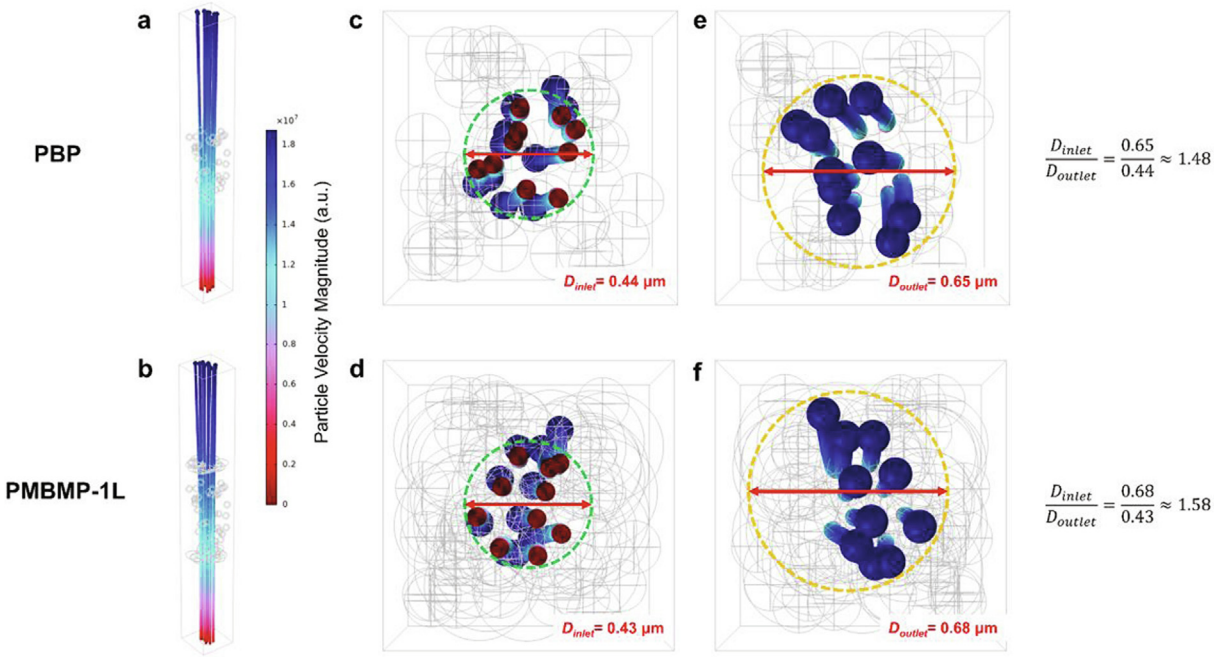

Fig. 5. Charged particle trajectory in 3D models of (a) PBP and (b) PMBMP-1L simulated by finite element method. The inlet locations (bottom electrode) of the charged particles in the model of (c) PBP and (d) PMBMP-1L, respectively. The outlet locations (top electrode) of the charged particles in the model of (e) PBP and (f) PMBMP-1L, respectively.

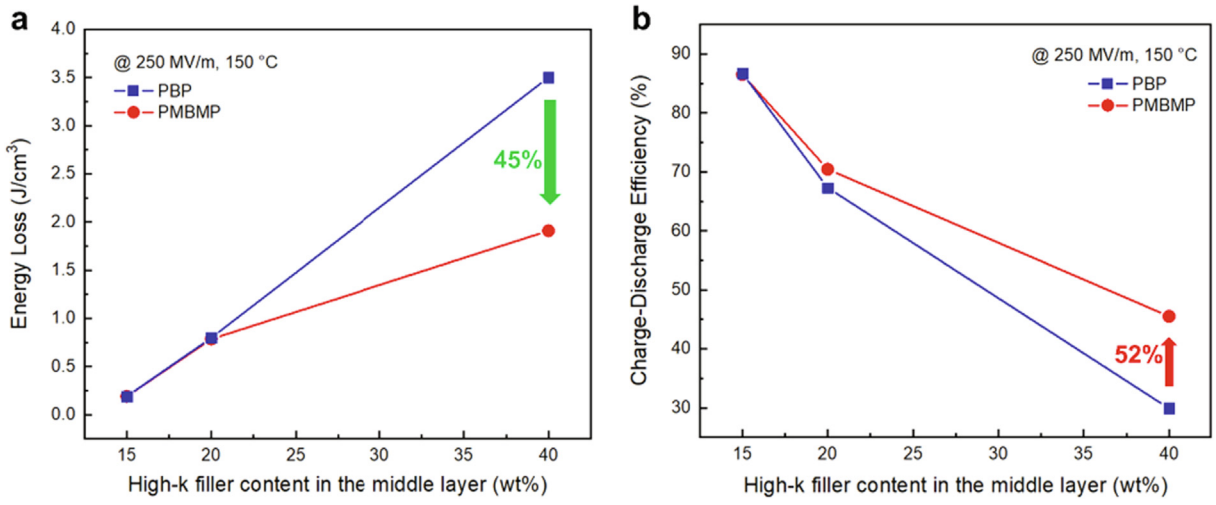

Fig. 6. (a) Energy losses and (b) charge-discharge efficiency of PBP and PMBMP-1L layered nanocomposites with the BT content varied from 15 wt% to 40 wt% in the middle layer at 150 °C.

multidisciplinary university research initiative (MURI) grant "Diagnosing and Impeding Dielectric Breakdown in Polymers" (N00014-17-1-2625).

Appendix A. Supplementary data

Supplementary data to this article can be found online at https://doi.org/10.1016/j.cej.2020.126093.

References

[1] Q. Tan, P. Irwin, Y. Cao, Advanced dielectrics for capacitors, IEEJ Trans. Fund. Mater. 126 (2006) 1153–1159.
[2] W.J. Sarjeant, J. Zirnheld, F.W. MacDougall, Capacitors, IEEE Trans. Plasma Sci. 26 (1998) 1368–1392.
[3] M.S. Whittingham, Materials challenges facing electrical energy storage, MRS Bull. 33 (2011) 411–419.
[4] E. Karden, S. Ploumen, B. Fricke, T. Miller, K. Snyder, Energy storage devices for future hybrid electric vehicles, J. Power Sources 168 (2007) 2–11.
[5] S. Luo, Y. Shen, S. Yu, Y. Wan, W.-H. Liao, R. Sun, C.-P. Wong, Construction of a 3D-$BaTiO_3$ network leading to significantly enhanced dielectric permittivity and energy storage density of polymer composites, Energy Environ. Sci. 10 (2017) 137–144.
[6] B. Chu, X. Zhou, K. Ren, B. Neese, M. Lin, Q. Wang, F. Bauer, Q.M. Zhang, A dielectric polymer with high electric energy density and fast discharge speed, Science 313 (2006) 334–336.
[7] Q. Wang, L. Zhu, Polymer nanocomposites for electrical energy storage, J. Polym. Sci. Part B 49 (2011) 1421–1429.
[8] L. Zhu, Exploring strategies for high dielectric constant and low loss polymer dielectrics, J. Phys. Chem. Lett. 5 (2014) 3677–3687.
[9] X. Zhang, Y. Shen, B. Xu, Q. Zhang, L. Gu, J. Jiang, J. Ma, Y. Lin, C.W. Nan, Giant energy density and improved discharge efficiency of solution-processed polymer nanocomposites for dielectric energy storage, Adv. Mater. 28 (2016) 2055–2061.
[10] Z.M. Dang, J.K. Yuan, S.H. Yao, R.J. Liao, Flexible nanodielectric materials with high permittivity for power energy storage, Adv. Mater. 25 (2013) 6334–6365.
[11] S. Ducharme, An inside-out approach to storing electrostatic energy, ACS Nano 3 (2009) 2447–2450.
[12] X. Huang, P. Jiang, Core-shell structured high-k polymer nanocomposites for energy storage and dielectric applications, Adv. Mater. 27 (2015) 546–554.

[13] H. Tang, Y. Lin, H.A. Sodano, Enhanced energy storage in nanocomposite capacitors through aligned PZT nanowires by uniaxial strain assembly, Adv. Energy Mater. 2 (2012) 469–476.
[14] V.K. Prateek, R.K. Thakur, Gupta, Recent progress on ferroelectric polymer-based nanocomposites for high energy density capacitors: synthesis, dielectric properties, and future aspects, Chem. Rev. 116 (2016) 4260–4317.
[15] Z. Pan, B. Liu, J. Zhai, L. Yao, K. Yang, B. Shen, $NaNbO_3$ two-dimensional platelets induced highly energy storage density in trilayered architecture composites, Nano Energy 40 (2017) 587–595.
[16] Q. Li, G. Zhang, F. Liu, K. Han, M.R. Gadinski, C. Xiong, Q. Wang, Solution-processed ferroelectric terpolymer nanocomposites with high breakdown strength and energy density utilizing boron nitride nanosheets, Energy Environ. Sci. 8 (2015) 922–931.
[17] Q. Li, L. Chen, M.R. Gadinski, S. Zhang, G. Zhang, U. Li, E. Iagodkine, A. Haque, L.Q. Chen, N. Jackson, Q. Wang, Flexible high-temperature dielectric materials from polymer nanocomposites, Nature 523 (2015) 576–579.
[18] Z. Zhang, D.H. Wang, M.H. Litt, L.S. Tan, L. Zhu, High-temperature and high-energy-density dipolar glass polymers based on sulfonylated poly(2,6-dimethyl-1,4-phenylene oxide), Angew. Chem. Int. Ed. Engl. 57 (2018) 1528–1531.
[19] M. Guo, J. Jiang, Z. Shen, Y. Lin, C.-W. Nan, Y. Shen, High-energy-density ferroelectric polymer nanocomposites for capacitive energy storage: enhanced breakdown strength and improved discharge efficiency, Mater. Today 29 (2019) 49–67.
[20] X. Zhang, Y. Shen, Q. Zhang, L. Gu, Y. Hu, J. Du, Y. Lin, C.W. Nan, Ultrahigh energy density of polymer nanocomposites containing $BaTiO_3$@TiO_2 nanofibers by atomic-scale interface engineering, Adv. Mater. 27 (2015) 819–824.
[21] M. Rabuffi, G. Picci, Status quo and future prospects for metallized polypropylene energy storage capacitors, IEEE Trans. Plasma Sci. 30 (2002) 1939–1942.
[22] B. Fan, F. Liu, G. Yang, H. Li, G. Zhang, S. Jiang, Q. Wang, Dielectric materials for high-temperature capacitors, IET Nanodielectr. 1 (2018) 32–40.
[23] A. Azizi, M.R. Gadinski, Q. Li, M.A. AlSaud, J. Wang, Y. Wang, B. Wang, F. Liu, L.Q. Chen, N. Alem, Q. Wang, High-performance polymers sandwiched with chemical vapor deposited hexagonal boron nitrides as scalable high-temperature dielectric materials, Adv. Mater. 29 (2017) 1701864.
[24] H. Li, D. Ai, L. Ren, B. Yao, Z. Han, Z. Shen, J. Wang, L.Q. Chen, Q. Wang, Scalable polymer nanocomposites with record high-temperature capacitive performance enabled by rationally designed nanostructured inorganic fillers, Adv. Mater. 31 (2019) 1900875.
[25] Y. Wang, J. Chen, Y. Li, Y. Niu, Q. Wang, H. Wang, Multilayered hierarchical polymer composites for high energydensity capacitors, J. Mater. Chem. A 7 (2019) 2965–2980.
[26] H. Luo, X. Zhou, C. Ellingford, Y. Zhang, S. Chen, K. Zhou, D. Zhang, C.R. Bowen, C. Wan, Interface design for high energy density polymer nanocomposites, Chem. Soc. Rev. 48 (2019) 4424–4465.
[27] J. Jiang, Z. Shen, J. Qian, Z. Dan, M. Guo, Y. Lin, C.-W. Nan, L. Chen, Y. Shen, Ultrahigh discharge efficiency in multilayered polymer nanocomposites of high energy density, Energy Storage Mater. 18 (2019) 213–221.
[28] Y.N. Hao, X.H. Wang, S. O'Brien, J. Lombardi, L.T. Li, Flexible $BaTiO_3$/PVDF gradated multilayer nanocomposite film with enhanced dielectric strength and high energy density, J. Mater. Chem. C 3 (2015) 9740–9747.
[29] F. Liu, Q. Li, J. Cui, Z. Li, G. Yang, Y. Liu, L. Dong, C. Xiong, H. Wang, Q. Wang, High-energy-density dielectric polymer nanocomposites with trilayered architecture, Adv. Funct. Mater. 27 (2017) 1606292.
[30] Y. Wang, J. Cui, Q. Yuan, Y. Niu, Y. Bai, H. Wang, Significantly enhanced breakdown strength and energy density in sandwich-structured barium titanate/poly (vinylidene fluoride) nanocomposites, Adv. Mater. 27 (2015) 6658–6663.
[31] Y. Wang, J. Cui, L. Wang, Q. Yuan, Y. Niu, J. Chen, Q. Wang, H. Wang, Compositional tailoring effect on electric field distribution for significantly enhanced breakdown strength and restrained conductive loss in sandwich-structured ceramic/polymer nanocomposites, J. Mater. Chem. A 5 (2017) 4710–4718.
[32] Q. Li, F. Liu, T. Yang, M.R. Gadinski, G. Zhang, L.Q. Chen, Q. Wang, Sandwich-structured polymer nanocomposites with high energy density and great charge-discharge efficiency at elevated temperatures, Proc. Natl. Acad. Sci. U.S.A. 113 (2016) 9995–10000.
[33] M. Negishi, K. Akada, K. Takizawa, Space charge accumulation in coating materials for motor windings under DC high voltage, in: 2012 IEEE International Conference on Condition Monitoring and Diagnosis, Bali, Indonesia, 2012, pp. 122–125.
[34] A.A. Guseinov, Electrical properties of montmorillonite studied together with the processes occurring under thermal activation, Izvestiya, Izv, Phys. Solid Earth 53 (2017) 845–854.
[35] J. Tokarský, L. Kulhánková, V. Stýskala, K. Mamulová Kutláková, L. Neuwirthová, V. Matějka, P. Čapková, High electrical anisotropy in hydrochloric acid doped polyaniline/phyllosilicate nanocomposites: effect of phyllosilicate matrix, synthesis pathway and pressure, Appl. Clay Sci. 80–81 (2013) 126–132.
[36] F. Ding, J. Liu, S. Zeng, Y. Xia, K.M. Wells, M.P. Nieh, L. Sun, Biomimetic nanocoatings with exceptional mechanical, barrier, and flame-retardant properties from large-scale one-step coassembly, Sci. Adv. 3 (2017) e1701212.
[37] P. Hu, W. Sun, M. Fan, J. Qian, J. Jiang, Z. Dan, Y. Lin, C.W. Nan, M. Li, Y. Shen, Large energy density at high-temperature and excellent thermal stability in polyimide nanocomposite contained with small loading of BaTiO3 nanofibers, Appl. Surf. Sci. 458 (2018) 743–750.
[38] W. Sun, X. Lu, J. Jiang, X. Zhang, P. Hu, M. Li, Y. Lin, C.W. Nan, Y. Shen, Dielectric and energy storage performances of polyimide/$BaTiO_3$ nanocomposites at elevated temperatures, J. Appl. Phys. 121 (2007) 244101.
[39] M.A. Marwat, B. Xie, Y. Zhu, P. Fan, K. Liu, M. Shen, M. Ashtar, S. Kongparakul, C. Samart, H. Zhang, Sandwich structure-assisted significantly improved discharge energy density in linear polymer nanocomposites with high thermal stability, Colloids Surf. A 581 (2019) 123802.
[40] Z.H. Shen, J.J. Wang, J.Y. Jiang, S.X. Huang, Y.H. Lin, C.W. Nan, L.Q. Chen, Y. Shen, Phase-field modeling and machine learning of electric-thermal-mechanical breakdown of polymer-based dielectrics, Nat. Commun. 10 (2019) 1843.
[41] K. Yu, Y. Niu, F. Xiang, Y. Zhou, Y. Bai, H. Wang, Enhanced electric breakdown strength and high energy density of barium titanate filled polymer nanocomposites, J. Appl. Phys. 114 (2013) 174107.
[42] V. Tomer, C.A. Randall, G. Polizos, J. Kostelnick, E. Manias, High- and low-field dielectric characteristics of dielectrophoretically aligned ceramic/polymer nanocomposites, J. Appl. Phys. 103 (2008) 034115.